Quantum transport in driven systems with vibrations: Floquet nonequilibrium Green's functions and the self-consistent Born approximation

Thomas D. Honeychurch and Daniel S. Kosov
College of Science and Engineering, James Cook University, Townsville, QLD, 4811, Australia

We investigate the effects of alternating voltage on nonequilibrium quantum systems with localized phonon modes. Nonequilibrium Green's functions are utilized, with electron-phonon coupling being considered with the *GD* approximation (self-consistent Born approximation). Using a Floquet approach, we assume periodicity of the dynamics. This approach allows us to investigate the influence of the driven electronic component on the nonequilibrium occupation of the vibrations. It was found that signatures of inelastic transport gained photon-assisted peaks. A simplistic model was proposed and found to be in good agreement with the full model in certain parameter ranges. Moreover, it was found that driving the alternating current at resonance with vibrational frequencies caused an increase in phonon occupation.

I. INTRODUCTION

The transport properties of quantum dots, especially molecular junctions, can be significantly altered by vibrations coupled to the central region, causing an array of interesting phenomena [1]. Of particular importance is how vibrations, often in conjunction with other phenomena, inhibit device functionality and stability.

Investigations that cast vibrations as localized phonons have been extensively studied under various parameter ranges. When coupling between electronic and vibrational components is sufficiently small, differential conductance through a junction has been found to vary due to changes in bias voltage, with electrons inelastically interacting with central phonons [1–3], explaining the experimental phenomena observed in inelastic electron tunneling spectroscopy and point contact spectroscopy experiments [4–6]. For sufficiently large coupling between electrons and phonons, transport through the system is suppressed due to the Franck-Condon blockade [1,7]. With semiclassical approaches to mechanical change within a junction, electron-friction and nonadiabatic effects with general potentials can be studied [8–13].

In steady state, vibrations within a molecular junction have been investigated with a variety of methods [14]. Nonequilibrium Green's functions approaches have been used to model vibrations within self-consistent perturbation theory [2,3,15,16], polaron and dressed tunneling approximations [17,18], equation-of-motion methods [19], and many more. Vibrations can also be studied with master equation approaches, like the Redfield master equations [20], or more involved methods like hierarchical quantum master equations [21]. Vibrations often contribute significantly to junction failure. With the current lifetime of many molecular junctions being, at best, only seconds long [22], tackling the problem a junction instability stands as a significant hurdle for the field [8,23].

The further addition of time dependence in the form of varying voltages and electric fields is frequent within the theory and experiment surrounding molecular electronics, allowing for the probing and control of dynamics within the junction. A prime example is recent work that has seen molecular junctions probed on picosecond time frames with a laser pulse-pair scheme [24]. Time-dependent potentials also allow for the realization of novel functionalities, including time-dependent molecular rectifiers [25,26] and molecular pumps [27]. Beyond static driving, molecular junctions are often studied within time-dependent settings, like transience [28,29], periodic driving of lead energies [30], couplings [31], or by laser pulses [32,33], when the central junction is subject to monochromatic electric fields [34], or within the limit of slow drivings [35,36].

Given the importance of vibrations, understanding their dynamics under various time-dependent scenarios will be essentials for molecular junction designs that seek to capitalize on time-dependent effects. Recently, exploration into the effects of time-dependent driving upon vibrations has been growing: transient dynamics of vibrationally active molecular junctions have been investigated theoretically with the self-consistent perturbation theory [37] and dressed tunneling approximation [38]; harmonic driving of gate voltages was used to increase current within the Franck-Condon blockade region [39]; vibrations with perturbatively slow driving have been investigated with mean field in a nonequilibrium Green's functions setting [35] and with hierarchical master equations [36]; and nonequilibrium Green's functions and linear response theory have been utilized to investigate conductance profiles and properties of phonons under small drivings [40–42].

Of particular interest is whether time-dependent driving can be used to reduce vibrations while still allowing for current flow comparable to the equivalent static case. This has been predicted with a master equation approach [20] and for

vibrations modeled semiclassically with a Langevin approach [43].

Within this paper we use a Floquet nonequilibrium Green's function approach to investigate the effects of time-periodic driving on a single-level electronic molecule coupled to a single phonon mode, making use of the self-consistent perturbation theory in the form of the *GD* approximation [29,37,44].

It was found that changes in conductance, indicative of inelastic electron transport spectroscopy, gain photon-assisted side peaks. Following intuition from photon-assisted transport and inelastic electron transport spectroscopy, a simplistic form for the current and phonon occupation is hypothesized and found to be a good match in limiting cases. It was also observed that resonances between the vibrational and driving frequencies resulted in increases to phonon occupation, with two different contributing mechanisms.

This paper is organized as follows: Section II covers the theory. In Sec. III, the method is applied to a single electronic level coupled with a phonon. In Sec. IV, the results of the paper are summarized. Atomic units are used throughout the paper.

II. THEORY

To describe electrons moving through a junction while interacting with central phonons, we make use of a nonequilibrium Green's functions approach, considering the electron-vibration coupling within the *GD* approximation, also known as the self-consistent Born approximation [44–46].

A. Hamiltonian

The system is modeled with the following Hamiltonian:

$$H(t) = H_{el}(t) + H_{vib} + H_{e-v}. \tag{1}$$

The electronic components are given by

$$H_{el}(t) = H_{central} + H_{leads}(t) + H_{coupling}, \tag{2}$$

$$H_{central}(t) = \sum_{ij} \epsilon_{ij} d_i^\dagger d_j, \tag{3}$$

$$H_{leads}(t) = \sum_{k,\alpha=L,R} \epsilon_{k\alpha}(t) c_{k\alpha}^\dagger c_{k\alpha}, \tag{4}$$

$$H_{coupling}(t) = \sum_{ik\alpha=L,R} t_{k\alpha i} \, c_{k\alpha}^\dagger d_i + \text{H.c.}, \tag{5}$$

and the Hamiltonian for the vibrations is given as

$$H_{vibratons} = \sum_{\alpha} \omega_\alpha a_\alpha^\dagger a_\alpha, \tag{6}$$

and the coupling between the electronic and vibrational components is given by

$$H_{e-v} = \sum_{ij,\alpha} \lambda_{i,j}^\alpha Q_\alpha d_i^\dagger d_j. \tag{7}$$

Here, d_i ($d_i^\dagger$) and $c_{k\alpha}$ ($c_{k\alpha}^\dagger$) are annihilation (creation) operators for site i in the central region and $k\alpha$ in the leads, respectively. For the phonons, the quantum operator for the position is given by $Q_\alpha = \frac{1}{\sqrt{2}}(a_\alpha + a_\alpha^\dagger)$ and the momentum

given by $P_\alpha = \frac{1}{\sqrt{2}i}(a_\alpha - a_\alpha^\dagger)$, where a_α ($a_\alpha^\dagger$) is the annihilation (creation) operator for the phonon α. Within the investigation, only the energies of the leads are considered to be time dependent. It is a simple extension to consider time dependence within the central energy levels ϵ_{ij} and couplings $t_{k\alpha,i}$.

B. Nonequilibrium Green's functions

To capture the dynamics of the system out of equilibrium, we make use of a nonequilibrium Green's function approach [45,47,48]. On the Keldysh contour, we have the electronic contour Green's function:

$$G_{ij}(\tau, \tau') = -i\langle T_c(d_i(\tau)d_j^\dagger(\tau'))\rangle. \tag{8}$$

Similarly, we have the phononic Green's functions,

$$\begin{aligned} D_{\alpha\beta}(\tau, \tau') &= -i\langle T_c(\Delta Q_\alpha(\tau)\Delta Q_\beta(\tau'))\rangle \\ &= -i[\langle T_c(Q_\alpha(\tau)Q_\beta(\tau'))\rangle - \langle Q_\alpha(\tau)\rangle\langle Q_\beta(\tau')\rangle] \end{aligned} \tag{9}$$

and

$$\begin{aligned} D_{\alpha\beta}^{PP}(\tau, \tau') &= -i\langle T_c(\Delta P_\alpha(\tau)\Delta P_\beta(\tau'))\rangle \\ &= -i[\langle T_c(P_\alpha(\tau)P_\beta(\tau'))\rangle - \langle P_\alpha(\tau)\rangle\langle P_\beta(\tau')\rangle], \end{aligned} \tag{10}$$

where $\Delta Q_\alpha(\tau) = Q_\alpha(\tau) - \langle Q_\alpha(\tau)\rangle$ and $\Delta P_\alpha(\tau) = P_\alpha(\tau) - \langle P_\alpha(\tau)\rangle$. The corresponding noninteracting Green's functions are denoted with lowercase lettering.

The current from the left or right lead is given by

$$\begin{aligned} I_\alpha(t) = 2\,\text{Re}\Big\{ \int_{-\infty}^{\infty} dt_1 \text{Tr}[G^<(t, t_1)\Sigma_\alpha^A(t_1, t) \\ + G^R(t, t_1)\Sigma_\alpha^<(t_1, t)] \Big\}, \end{aligned} \tag{11}$$

and the occupation of the electrons within the central region is given by

$$n_i^{el}(t) = -iG_{ii}^<(t, t). \tag{12}$$

For the phonons, we are principally interested in the phonon occupation:

$$\begin{aligned} n_\alpha^{ph}(t) &= \langle a_\alpha^\dagger(t)a_\alpha(t)\rangle = \frac{1}{2}[\langle P_\alpha(t)^2\rangle + \langle Q_\alpha(t)^2\rangle] - \frac{1}{2} \\ &= \frac{1}{2}[iD_{\alpha\alpha}^<(t, t) + \langle Q_\alpha(t)\rangle^2 + iD_{\alpha\alpha}^{<,PP}(t, t) + \langle P_\alpha(t)\rangle^2] \\ &\quad - \frac{1}{2}. \end{aligned} \tag{13}$$

C. Equations of motion

To calculate the electronic and phononic nonequilibrium Green's functions, we use the Kadanoff-Baym equations:

$$\begin{aligned} i\frac{\partial}{\partial \tau}G_{ij}(\tau, \tau') - \sum_k \epsilon_{ik} G_{kj}(\tau, \tau') \\ - \sum_k \int_c d\tau_1 \Sigma_{ik}(\tau, \tau_1)G_{kj}(\tau_1, \tau') = \delta_{ij}\delta_c(\tau - \tau') \end{aligned} \tag{14}$$

and

$$\frac{-1}{\omega_\alpha}\left(\frac{d^2}{d\tau^2} + \omega_\alpha^2\right)D_{\alpha\beta}(\tau, \tau')$$

$$= \delta_c(\tau - \tau')\delta_{\alpha\beta} + \sum_\gamma \int d\tau_1 \Pi_{\alpha\gamma}(\tau, \tau_1)D_{\gamma\beta}(\tau_1, \tau'). \quad (15)$$

Here the external influences on the central electrons and phonons is captured in $\Sigma_{ij}(\tau, \tau')$ and $\Pi_{\alpha\beta}(\tau, \tau')$, respectively. The collective influence on the central regions electrons can be separated into that due to the phonons and the leads,

$$\Sigma(\tau, \tau') = \Sigma_{int}(\tau, \tau') + \Sigma_{leads}(\tau, \tau'), \quad (16)$$

and, similarly for the phonons,

$$\Pi(\tau, \tau') = \Pi_{int}(\tau, \tau') + \Pi_{bath}(\tau, \tau'). \quad (17)$$

Calculating the electronic lead self-energies follows the standard procedure:

$$\Sigma_{\alpha,ij}^{<,>,R,A}(t, t') = \sum_{k,k'} t_{k\alpha,i}^*(t) \, g_{k\alpha,k'\alpha}^{<,>,R,A}(t, t')t_{k'\alpha,j}(t'), \quad (18)$$

where the noninteracting lead self-energies follow the standard definitions,

$$g_{k\alpha,k'\alpha'}^<(t, t') = if_{k\alpha}e^{-i\int_{t'}^t dt_1 \epsilon_{k\alpha}(t_1)}\delta_{k,k'}, \quad (19)$$

$$g_{k\alpha,k'\alpha}^>(t, t') = -i(1 - f_{k\alpha})e^{-i\int_{t'}^t dt_1 \epsilon_{k\alpha}(t_1)}\delta_{k,k'}, \quad (20)$$

$$g_{k\alpha,k'\alpha}^R(t, t') = -i\Theta(t - t')e^{-i\int_{t'}^t dt_1 \epsilon_{k\alpha}(t_1)}\delta_{k,k'}, \quad (21)$$

$$g_{k\alpha,k'\alpha}^A(t, t') = i\Theta(t' - t)e^{-i\int_{t'}^t dt_1 \epsilon_{k\alpha}(t_1)}\delta_{k,k'}. \quad (22)$$

The time dependence takes the form $\epsilon_{k\alpha}(t) = \epsilon_{k\alpha} + \phi_\alpha(t)$, which allows us to separate out the phase induced by the varying energies of the leads from rest of the self-energy:

$$\Sigma_{\alpha,ij}(t, t') = \Sigma_{\alpha,ij}'(t - t')e^{-i\int_{t'}^t dt_1 \phi_\alpha(t_1)}$$

$$= e^{-i\Phi_\alpha(t)}\Sigma_{\alpha,ij}'(t - t')e^{i\Phi_\alpha(t')}, \quad (23)$$

where $\Phi_\alpha(t)$ is the antiderivative of $\phi_\alpha(t)$, and $\Sigma_{\alpha,ij}'(t - t')$ is the self-energy of the equivalent static case, which is taken in the wide-band approximation:

$$\Sigma_{\alpha,ij}^{A/R}(\omega) = \pm\frac{i}{2}\Gamma_{\alpha,ij}, \quad (24)$$

$$\Sigma_{\alpha,ij}^<(\omega) = if_\alpha(\omega)\Gamma_{\alpha,ij}, \quad (25)$$

and

$$\Sigma_{\alpha,ij}^>(\omega) = -i(1 - f_\alpha(\omega))\Gamma_{\alpha,ij}, \quad (26)$$

where the Fermi-Dirac occupation is given by

$$f_{k\alpha} = \frac{1}{1 + e^{(\epsilon_{k\alpha} - \mu_\alpha)/T_\alpha}}. \quad (27)$$

Within the investigation, the lead energies were driven sinusoidally,

$$\phi_\alpha(t) = \Delta_\alpha \cos(\Omega_\alpha t), \quad (28)$$

which gives $\Phi(t) = (\Delta_\alpha/\Omega_\alpha)\sin(\Omega_\alpha t)$, which can be expressed as a Fourier series with the Jacobi-Anger

expansion:

$$e^{i\frac{\Delta_\alpha}{\Omega_\alpha}\sin(\Omega_\alpha t)} = \sum_{n=-\infty}^{n=\infty} J_n\left(\frac{\Delta_\alpha}{\Omega_\alpha}\right)e^{in\Omega_\alpha t}, \quad (29)$$

where $J_n(x)$ are Bessel functions of the first kind.

For the noninteracting phonons, we have the following phonon Green's functions:

$$d_{\alpha\beta}^R(\omega) = \left[\frac{\frac{1}{2}}{\omega - \omega_\alpha + i\eta_\alpha} - \frac{\frac{1}{2}}{\omega + \omega_\alpha + i\eta_\alpha}\right]\delta_{\alpha\beta}, \quad (30)$$

$$d_{\alpha\beta}^A(\omega) = \left[\frac{\frac{1}{2}}{\omega - \omega_\alpha - i\eta_\alpha} - \frac{\frac{1}{2}}{\omega + \omega_\alpha - i\eta_\alpha}\right]\delta_{\alpha\beta}, \quad (31)$$

$$d_{\alpha\beta}^<(\omega) = -\pi i[f_B(\omega_\alpha)\delta(\omega - \omega_\alpha) + (1 + f_B(\omega_\alpha))\delta(\omega + \omega_\alpha)]\delta_{\alpha\beta}, \quad (32)$$

$$d_{\alpha\beta}^>(\omega) = -\pi i[f_B(\omega_\alpha)\delta(\omega + \omega_\alpha) + (1 + f_B(\omega_\alpha))\delta(\omega - \omega_\alpha)]\delta_{\alpha\beta}. \quad (33)$$

Instead of letting η_α be infinitesimals, we take them as finite so as to capture the influence of a phonon bath on central phonons. Making use of fluctuation-dissipation relations, we can introduce η_α into the lesser and greater phonon Green's functions:

$$d_\alpha^<(\omega) = \left(d_\alpha^R(\omega) - d_\alpha^A(\omega)\right)f_B(\omega)$$

$$= \left(-\frac{i\eta_\alpha}{(\omega - \omega_\alpha)^2 + \eta_\alpha^2} + \frac{i\eta_\alpha}{(\omega + \omega_\alpha)^2 + \eta_\alpha^2}\right)f_B(\omega) \quad (34)$$

and

$$d_\alpha^>(\omega) = \left(d_\alpha^R(\omega) - d_\alpha^A(\omega)\right)(1 + f_B(\omega))$$

$$= \left(-\frac{i\eta_\alpha}{(\omega - \omega_\alpha)^2 + \eta_\alpha^2} + \frac{i\eta_\alpha}{(\omega + \omega_\alpha)^2 + \eta_\alpha^2}\right) \times (1 + f_B(\omega)), \quad (35)$$

where taking the limit of η,

$$\lim_{\eta\to 0^+}\left[\frac{\eta}{(\omega - \omega_0)^2 + \eta^2}\right] \to \pi\delta(\omega - \omega_0), \quad (36)$$

and substituting for $f_B^0(-\omega) = -(f_B^0(\omega) + 1)$ gives us back Eqs. (32) and (33).

For the lesser and greater phonon Green's functions, we can use the fluctuation-dissipation rules to cast the effects due to the infinitesimals as self-energies. Equating Eqs. (32) and (33) with the associated Keldysh equations gives us

$$\Pi_\alpha^{</>}(\omega) = \mp 4i\eta_\alpha\left(\frac{\omega}{\omega_\alpha}\right)f_B(\pm\omega). \quad (37)$$

This phonon self-energy is used to incorporate the effects of the infinitesimal into self-consistent calculations [see Eq. (17)].

In addition to the above Green's functions, we need to calculate $\langle Q_\alpha(\tau)\rangle$, $\langle P_\alpha(\tau)\rangle$, and $D_{\alpha,\alpha'}^{PP}(\tau, \tau')$, allowing for the calculation of the phonon occupation. The equation of motion

for the average position is given as [45]

$$\frac{-1}{\omega_\alpha}\left(\frac{d^2}{d\tau^2} + \omega_\alpha^2\right)\langle Q_\alpha(\tau)\rangle$$

$$= \sum_{ij} -i\lambda_{ij}^\alpha G_{ji}(\tau, \tau^+)$$

$$+ \int d\tau_1 \Pi_\alpha^{bath}(\tau, \tau_1)\langle Q_\alpha(\tau_1)\rangle. \quad (38)$$

For the terms with momentum operators, we make use of

$$\frac{d}{d\tau}Q_\alpha(\tau) = \omega_\alpha P_\alpha(\tau), \quad (39)$$

which gives us the equations of motions,

$$\frac{d}{d\tau}\langle Q_\alpha(\tau)\rangle = \omega_\alpha \langle P_\alpha(\tau)\rangle \quad (40)$$

and

$$\frac{d}{d\tau d\tau'}D_{\alpha\beta}(\tau, \tau') = \omega_\alpha \delta_{\alpha\beta}\delta(\tau, \tau') + D_{\alpha\beta}^{PP}(\tau, \tau')\omega_\alpha\omega_\beta. \quad (41)$$

These objects allow us to calculate occupation:

$$n_\alpha^{ph}(\tau) = \langle T_c(a_\alpha(\tau)a_\alpha^\dagger(\tau^+))\rangle = \frac{1}{2}\left[\langle T_c(Q_\alpha^2(\tau))\rangle\right.$$

$$+ \langle T_c(P_\alpha^2(\tau))\rangle\left.\right] - \frac{1}{2}$$

$$= \frac{1}{2}[iD_{\alpha\alpha}(\tau, \tau^+) + \langle Q_\alpha(\tau)\rangle^2 + iD_{\alpha\alpha}^{PP}(\tau, \tau^+)$$

$$+ \langle P_\alpha(\tau)t\rangle^2] - \frac{1}{2}. \quad (42)$$

The interaction between electrons and phonons can be approximated within the *GD* approximation [44,46]:

$$\mathbf{\Sigma}_{ij}^{int}(\tau, \tau') = \mathbf{\Sigma}_{ij}^{har}(\tau, \tau') + \mathbf{\Sigma}_{ij}^{XC}(\tau, \tau'), \quad (43)$$

where

$$\mathbf{\Sigma}_{ij}^{har}(\tau, \tau') = -i\delta(\tau, \tau')\sum_\beta \lambda_{ij}^\beta \int_c d\tau_1 d_\beta(\tau, \tau_1)$$

$$\times \sum_{ml} \lambda_{ml}^\beta G_{lm}(\tau_1, \tau_1^+), \quad (44)$$

$$\mathbf{\Sigma}_{ij}^{XC}(\tau, \tau') = i\sum_{\mu\nu,ml} D_{\mu\nu}(\tau, \tau')\lambda_{im}^\mu G_{ml}(\tau, \tau')\lambda_{lj}^\nu, \quad (45)$$

and

$$\Pi_{\alpha\beta}^{int}(\tau, \tau') = -i\sum_{mlkp} \lambda_{ml}^\alpha G_{lk}(\tau, \tau')\lambda_{kp}^\beta G_{pm}(\tau', \tau). \quad (46)$$

D. Floquet theory

Moving the equations of motion from the contour to real time with the greater, lesser, retarded, and advanced projections [47,49], we can solve the equations of motion with a Floquet approach [30,50], where we assume that the system is time periodic around the central time $T = \frac{t+t'}{2}$ and complete a Fourier transform with respect to the relative time, $\tau = t - t'$:

$$A(t, t') = A(T, \tau) = \sum_{n=-\infty}^{\infty} A(\tau, n)e^{\Omega inT} \quad (47)$$

and

$$A(\omega, n) = \frac{1}{P}\int_0^P dT \ e^{-i\Omega nT}\int_{-\infty}^{\infty} d\tau e^{i\omega\tau} A(T, \tau). \quad (48)$$

For solving the convolutions of the form

$$C(t, t') = \int dt_1 A(t, t_1)B(t_1, t'), \quad (49)$$

we recast the Fourier coefficients into a Floquet matrix,

$$\bar{A}(\omega, m, n) = A\left(\omega + \frac{\Omega}{2}(m+n), n-m\right), \quad (50)$$

which allows us to express the convolution as a matrix multiplication,

$$\bar{C}(\omega, m, n) = \sum_{r=-\infty}^{\infty} \bar{A}(\omega, m, r)\bar{B}(\omega, r, n), \quad (51)$$

allowing for the Kadanoff-Baym equations to be written as a matrix equation:

$$(\omega + \Omega m)\bar{G}_{ij}^{R/A}(\omega, m, n) - \sum_k \epsilon_{ik}\bar{G}_{kj}^{R/A}(\omega, m, n)$$

$$= \delta_{ij}\delta_{mn} + \sum_{k,r} \bar{\Sigma}_{ik}^{R/A}(\omega, m, r)\bar{G}_{kj}^{R/A}(\omega, r, n), \quad (52)$$

$$\bar{G}_{ij}^<(\omega, m, n) = \sum_{kw,rs} \bar{G}_{ik}^R(\omega, m, r)\bar{\Sigma}_{kw}^<(\omega, r, s)$$

$$\times \bar{G}_{wj}^A(\omega, s, n), \quad (53)$$

$$\frac{-1}{\omega_\alpha}\left(\omega_\alpha^2 - (\omega + \Omega m)^2\right)\bar{D}_{\alpha\beta}^R(\omega, m, n)$$

$$= \delta_{\alpha\beta}\delta_{mn} + \sum_{\gamma,r} \bar{\Pi}_{\alpha\gamma}(\omega, m, r)\bar{D}_{\gamma\beta}(\omega, r, n), \quad (54)$$

$$\bar{D}_{\alpha\beta}^<(\omega, m, n)$$

$$= \sum_{\nu\gamma,rs} \bar{D}_{\alpha\nu}^R(\omega, m, r)\bar{\Pi}_{\nu\gamma}^<(\omega, r, s)\bar{D}_{\gamma\beta}^A(\omega, s, n). \quad (55)$$

Other important objects transform in a similar manner. The lead self-energies, Eq. (23), making use of Eqs. (29) and (51), transform to

$$\bar{\Sigma}_{\alpha,ij}(\omega, m, n) = \sum_{pq,lk} \bar{S}_\alpha(m, p)\bar{\Sigma}'_{\alpha,lk}(\omega, p, q)\bar{S}_\alpha(n, q), \quad (56)$$

where $\bar{S}_\alpha(m, n) = J_{m-n}(\Delta_\alpha/\Omega_\alpha)$. The Fourier coefficients of the current and occupation can be taken from the Floquet matrices derived from Eqs. (11) and (12):

$$I_\alpha(n - m) = \bar{I}_\alpha(m, n)$$

$$= 2\int_{-\infty}^{\infty} \frac{d\omega}{2\pi}\sum_{r,ij}\left[\bar{G}_{ij}^R(\omega, m, r)\bar{\Sigma}_{ji}^<(\omega, r, n)\right.$$

$$+ \bar{G}_{ij}^<(\omega, m, r)\bar{\Sigma}_{ji}^R(\omega, r, n)\left.\right] \quad (57)$$

and

$$n_j^{el}(n - m) = \bar{n}_j^{el}(m, n) = -i\int_{-\infty}^{\infty} \frac{d\omega}{2\pi}\bar{G}_{jj}^<(\omega, m, n). \quad (58)$$

The time-resolved observables can then be found with Eq. (47), where $t \to t'$, and by taking only the real part, as per Eqs. (12) and (11).

Unfortunately, the interaction self-energies cannot be brought to such an amenable form and must be calculated from the Fourier coefficients. The interaction self-energies follow the forms

$$C_{XC}(t, t') = A(t, t')B(t, t'), \tag{59}$$

$$C_{POL}(t, t') = A(t, t')B(t', t), \tag{60}$$

$$C_{HAR}(t, t') = \delta(t - t') \int_{-\infty}^{\infty} dt_1 A(t, t_1)B(t_1, t_1). \tag{61}$$

Applying the Floquet transformation to the above gives

$$C_{XC}(\omega, n) = \sum_{m=-\infty}^{\infty} \int \frac{d\omega'}{2\pi} A(\omega', m)B(\omega - \omega', n - m), \tag{62}$$

$$C_{POL}(\omega, n) = \sum_{m=-\infty}^{\infty} \int \frac{d\omega'}{2\pi} A(\omega', m)B(\omega' - \omega, n - m), \tag{63}$$

and

$$C_{HAR}(\omega, n) = \sum_{m=-\infty}^{\infty} A\left(-\frac{\Omega}{2}(n + m), n - m\right)B'(n). \tag{64}$$

The $C_{HAR}(\omega, n)$ simplifies when $A(t, t') = A(t - t')$, giving us

$$C_{HAR}(\omega, n) = \sum_{m=-\infty}^{\infty} \delta_{m,n} A\left(-\frac{\Omega}{2}(m + n), 0\right)B(n)$$
$$= A(-\Omega n, 0)B(n). \tag{65}$$

The above allow us to cast the interaction self-energies in terms of their Fourier coefficients:

$$\Sigma_{har,ij}^{R}(\omega, r) = -i \sum_{\beta} \lambda_{ij}^{\beta} d_{\beta}^{R}(\omega = -\Omega r) \int \frac{d\omega}{2\pi}$$
$$\times \sum_{kw} \lambda_{kw}^{\beta} G_{wk}^{<}(\omega, r) \tag{66}$$

$$\Sigma_{XC,ij}^{R}(\omega, r) = \int \frac{d\omega'}{2\pi} \sum_{n=-\infty}^{\infty} \sum_{\mu\nu,ml}$$
$$\times iD_{\mu\nu}^{<}(\omega', n)\lambda_{im}^{\mu} G_{ml}^{R}(\omega - \omega', r - n)\lambda_{lj}^{\nu}$$
$$+ iD_{\mu\nu}^{R}(\omega', n)\lambda_{im}^{\mu} G_{ml}^{<}(\omega - \omega', r - n)\lambda_{lj}^{\nu}$$
$$+ iD_{\mu\nu}^{R}(\omega', n)\lambda_{im}^{\mu} G_{ml}^{R}(\omega - \omega', r - n)\lambda_{lj}^{\nu} \tag{67}$$

$$\Sigma_{XC,ij}^{<}(\omega, r) = \int \frac{d\omega'}{2\pi} \sum_{n=-\infty}^{\infty} \sum_{\mu\nu,ml}$$
$$\times iD_{\mu\nu}^{<}(\omega', n)\lambda_{im}^{\mu} G_{ml}^{<}(\omega - \omega', r - n)\lambda_{lj}^{\nu} \tag{68}$$

$$\Sigma_{XC,ij}^{>}(\omega, r) = \int \frac{d\omega'}{2\pi} \sum_{n=-\infty}^{\infty} \sum_{\mu\nu,ml}$$
$$\times iD_{\mu\nu}^{>}(\omega', n)\lambda_{im}^{\mu} G_{ml}^{>}(\omega - \omega', r - n)\lambda_{lj}^{\nu} \tag{69}$$

$$\Pi_{\alpha\beta}^{R}(\omega, r) = \int \frac{d\omega'}{2\pi} \sum_{n=-\infty}^{\infty} \sum_{mlkp}$$
$$- i\lambda_{ml}^{\alpha} G_{lk}^{<}(\omega', n)\lambda_{kp}^{\beta} G_{pm}^{A}(\omega' - \omega, r - n)$$
$$- i\lambda_{ml}^{\alpha} G_{lk}^{R}(\omega', n)\lambda_{kp}^{\beta} G_{pm}^{<}(\omega' - \omega, r - n) \tag{70}$$

$$\Pi_{\alpha\beta}^{<}(\omega, r) = \int \frac{d\omega'}{2\pi} \sum_{n=-\infty}^{\infty} \sum_{mlkp}$$
$$- i\lambda_{ml}^{\alpha} G_{lk}^{<}(\omega', n)\lambda_{kp}^{\beta} G_{pm}^{>}(\omega' - \omega, r - n) \tag{71}$$

$$\Pi_{\alpha\beta}^{>}(\omega, r) = \int \frac{d\omega'}{2\pi} \sum_{n=-\infty}^{\infty} \sum_{mlkp}$$
$$- i\lambda_{ml}^{\alpha} G_{lk}^{>}(\omega', n)\lambda_{kp}^{\beta} G_{pm}^{<}(\omega' - \omega, r - n). \tag{72}$$

Solving Eq. (38), we can cast the average phonon positions, and the subsequent average phonon momenta, in terms of Fourier coefficients

$$\langle Q_{\alpha}\rangle(r) = -id_{\alpha}^{R}(\omega = -\Omega r) \int \frac{d\omega}{2\pi} \sum_{ml} \lambda_{ml}^{\alpha} G_{lm}^{<}(\omega, r), \tag{73}$$

$$\langle P_{\alpha}\rangle(r) = \frac{ir\Omega}{\omega_0} \langle Q_{\alpha}\rangle(r). \tag{74}$$

We can complete a similar process for the phonon momentum Green's functions, allowing us to calculate variance of the momentum operators:

$$\langle (\Delta P_{\alpha})^2\rangle(r) = iD_{\alpha\alpha}^{PP,<}(r)$$
$$= \frac{i}{\omega_0^2} \int \frac{d\omega}{2\pi} \left[\omega^2 - \left(\frac{r\Omega}{2}\right)^2\right] D_{\alpha\alpha}^{<}(\omega, r). \tag{75}$$

E. Implementation

Solving for the Green's functions, the dimensions of the Floquet matrices and the corresponding Fourier series need to be truncated. The addition of more Fourier coefficients leads to more accurate results, converging on the exact result. Calculating the integrand of the Fourier coefficients was completed with an equidistant grid of points. Completing this procedure for the noninteracting case, the Floquet matrices were unraveled to Fourier coefficients using Eq. (50). The terms where $n + m = 0, -1$ of $\bar{A}(\omega, m, n)$ were taken for calculating the Fourier coefficients. These were then used to calculate the interaction self-energies before being reassembled into the Floquet matrices. The process was then completed iteratively, with convergence given by the Fourier coefficients of the phonon and electron occupations:

$$\frac{\sum_m |n_m^{k+1} - n_m^k|}{\sum_m |n_m^k|} \leqslant \delta, \tag{76}$$

where n_m^k is the kth iteration of the mth Fourier coefficient of the occupation in question, with δ as the convergence.
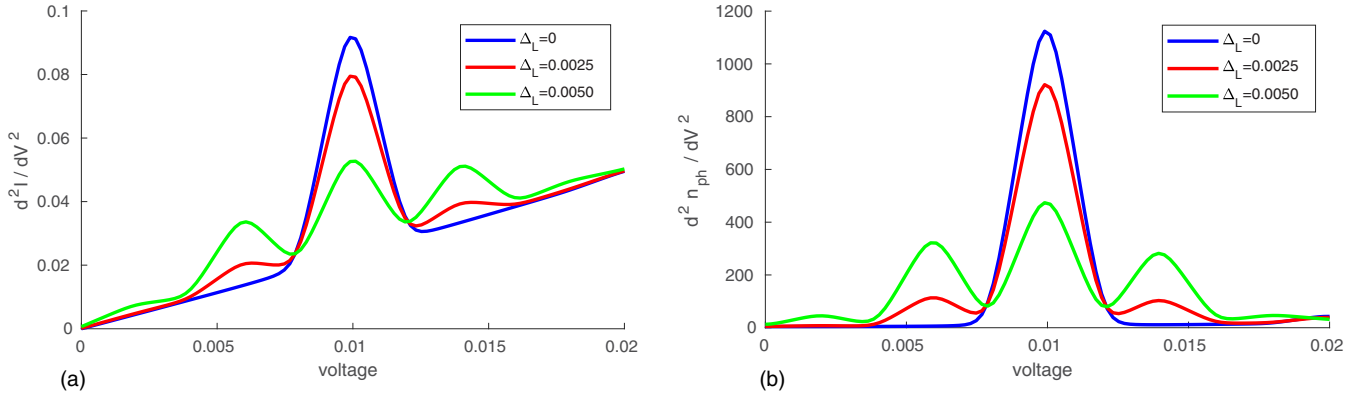
FIG. 1. The changes in d^2I/dV^2 and d^2n_{ph}/dV^2 as voltage increases, given different driving energies Δ_L. The other parameters are $\Gamma_L = \Gamma_R = 0.015$, $\epsilon_c = 0.1$, $\eta_c = 3 \times 10^{-5}$, $\Omega = 0.004$, $\omega_c = 0.01$, $\lambda_c = 0.015$, and $T = 1.5 \times 10^{-4}$. The bounds of the integrand were taken at -0.3 and 0.3. Fourier coefficients ranging from -8 to 8 were used in the calculation. The uniform grid spacing was 2×10^{-5}. The convergence was below 10^{-6} for both the electronic and phonon occupation.

III. RESULTS

For simplicity, we focus on a single electronic level coupled to a single phonon mode, with driving within the left lead:

$$
\begin{aligned}
H(t) = {} & \epsilon_c d^\dagger d + \sum_{ik\alpha=L,R} t_{k\alpha i} c_{k\alpha}^\dagger d + t_{k\alpha i}^* d^\dagger c_{k\alpha} \\
& + \sum_k (\epsilon_{kL} + \Delta_L \cos(\Omega t)) c_{kL}^\dagger c_{kL} \\
& + \epsilon_{kR} c_{kR}^\dagger c_{kR} + \omega_c a^\dagger a + \lambda_c Q d^\dagger d.
\end{aligned}
\tag{77}
$$

The parameters for the model consist of ϵ_c, the energy of the central level ω_c, the vibrational frequency of the phonon mode Ω, the driving frequency of the left lead Δ_L, the magnitude of the driving in the left lead $\Gamma_{L/R}$, the couplings to the leads λ_c, the coupling strength between the central level and phonon η_c, the coupling of the phonon to its bath, and the temperature of both leads T. Within the calculations, the driving frequency of the left lead is used as the frequency for the system's periodicity.

For the time-averaged picture of this model, we have two important limiting cases in the static, interacting case and the noninteracting case. The static case is well understood and extensively studied [1–3,14]. In this context, the phonon mode causes elastic corrections and facilitates new, inelastic channels of transport through the junction by means of absorption or emission of phonons. The latter only occurs when the voltage window widens to accommodate electrons that enter the junction before absorbing (emitting) a phonon of energy. The addition of extra channels through junction can be seen in subtle changes to the current, captured as peaks in the derivative of the differential conductance with respect to voltage.

The noninteracting case has also been extensively studied and can be explained with the notion of photon-assisted transport [47,51,52]. The periodic driving of the system (environment) results in contributions to the time-averaged observables from the equivalent static cases, with the driven energies shifted by integer multiples of the driving frequency of the time dependence. This can be interpreted as a

proportion of the electrons emitting or absorbing quanta of the energy, and hence the name photon-assisted transport. For the driving used in this paper, see Eq. (28), limited to the left lead we have

$$
\frac{1}{P} \int_0^P I_\alpha(t)\,dt = \sum_{n=-\infty}^{n=\infty} \left[J_n\!\left(\frac{\Delta_\alpha}{\Omega_\alpha}\right) \right]^2 I_\alpha^{DC}(\mu_L + n\Omega, \mu_R),
\tag{78}
$$

where $I_\alpha(t)$ is the AC-driven current through lead α and I_a^{DC} is the static case, where no driving is present.

Within certain parameter regimes, combining the reasoning from both limiting cases explains the features observed in the full model. In Fig. 1(a) we see the primary peak within dI^2/dV^2, indicative of inelastic collisions, gain additional satellite peaks due to absorption (emission) of quanta of energy by the electrons, prior to entering the junction, per photon-assisted tunneling. A similar effect is observed within Fig. 1(b), with d^2n_{ph}/dV^2 gaining photon-assisted side peaks, suggesting that the photon-assisted side peaks of the left lead contribute to the occupation of the phonon independently of each other.

The above insights suggest a simplistic model where Eq. (78) is augmented, with the static components being calculated with the addition of electron-phonon interactions. This method was often found to successfully predict the inelastic features of the full model. See Fig. 2 for an example, where the contributions given by Eq. (78) are plotted alongside the full and simplistic methods. The convergence for the simplistic model was calculated by using the average occupation as if it were static.

The simplistic model can be motivated for situations where the timescales for interaction between the electronic and phononic components, $t_\lambda \sim 1/\lambda_c$, is far longer than the traversal time for the electrons within the junction [1]:

$$
\frac{1}{\lambda_c} \gg \frac{1}{\sqrt{\Gamma^2 + \Delta E^2}},
\tag{79}
$$

where $\Gamma = \Gamma_L + \Gamma_R$, and ΔE, the injection energy, is the distance of the energy level from resonance, usually taken as the difference between the energy level and closest chemical
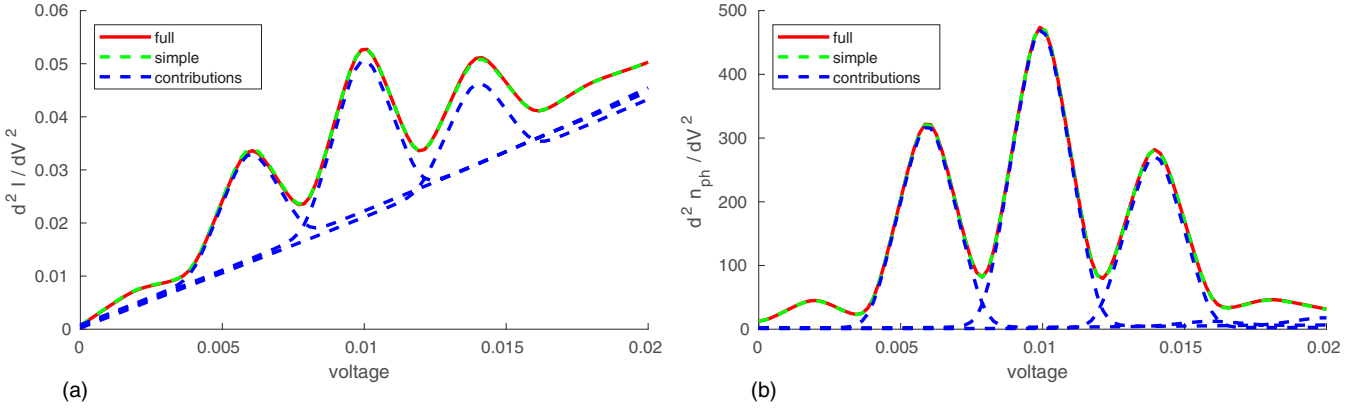
FIG. 2. The changes in d^2I/dV^2 and d^2n_{ph}/dV^2 as voltage increases. Here the full method is plotted alongside the simplistic method and contributions from $n = -1, 0, 1$ of Eq. (78). The other parameters are $\Gamma_L = \Gamma_R = 0.015$, $\epsilon_c = 0.1$, $\eta_c = 3 \times 10^{-5}$, $\Omega = 0.004$, $\omega_c = 0.01$, $\lambda_c = 0.015$, $\Delta_L = 0.005$, and $T = 1.5 \times 10^{-4}$. The bounds of the integrands were taken at -0.3 and 0.3. Fourier coefficients ranging from-8 to 8 were used in the calculation. The uniform grid spacing was 2×10^{-5}. The convergence was below 10^{-6} for both the electronic and phonon occupations.

potential. In the regime specified by the above assumption, the phonon mode will see the time dependence of the electronic component averaged over the long interaction time, hence the ability of the simplistic model to capture the dynamics. This insight is similar to that used to investigate the effects of AC driving with master equations [20,53], where weak coupling between the central region and leads results in the central region seeing an average picture of the leads' dynamics.

Within the model in question, it was found that resonance driving at $\Omega \approx \omega_c$ resulted in significant variations for several parameter ranges (see Figs. 3 and 4). This is mostly due to the sensitivity of the average position to resonant driving, which in turn influences the other observables. This can be seen in Fig. 3(c). This sensitivity to resonance comes from Eq. (73), for which the single-level case simplifies to

$$\langle Q \rangle(m) = \lambda_c \, d^R(-\Omega m) n_{el}(m). \quad (80)$$

Focusing on the bare, retarded phonon Green's function, we can separate out the real and imaginary parts:

$$d^R(\omega) = \frac{i}{2} \left(\frac{-\eta_c}{(\omega - \omega_c)^2 + \eta_c^2} + \frac{\eta_c}{(\omega + \omega_c)^2 + \eta_c^2} \right) + \frac{1}{2} \left(\frac{\omega - \omega_c}{(\omega - \omega_c)^2 + \eta_c^2} + \frac{\omega_c + \omega}{(\omega_c + \omega)^2 + \eta_c^2} \right). \quad (81)$$

The real and imaginary components of above are maximized around $\pm \Omega n \approx \omega_c$, especially when $\eta_c \ll \omega_c$. This results in the average phonon position being sensitive to periodic variation in the electronic occupation, resulting in the primary resonance peak, seen in Figs. 3(g), 3(h), and 4(b), around $\Omega \approx \omega_c$. Additionally, smaller subharmonic resonances can also be observed, see Figs. 3(g) and 4(a), which indicates the existence of higher-order Fourier coefficients in the electronic site's occupation.

In addition to the resonance at $\Omega \approx \omega_c$, a higher, smaller resonance was observed at $\Omega \approx 2\omega_c$, see Figs. 3(e), 3(f), 3(g), and 3(h). In contrast to resonance at $\Omega \approx \omega_c$, the resonance at $\Omega \approx 2\omega_c$ is due to increases in the variance of the phonon's

position and momentum, which is calculated with the phonon lesser GF. This can be seen in Fig. 3(h), where the contributions from Eq. (13) are separated into the contributions from the mean position and momenta, $\langle Q_\alpha(t) \rangle^2 + \langle P_\alpha(t) \rangle^2$, and the variance terms, $iD_{\alpha\alpha}^<(t, t) + iD_{\alpha\alpha}^{<,PP}(t, t)$.

Within the parameter ranges investigated, the time-resolved observables were found be explained primarily by the first- and second-order Fourier coefficients. For the resonances at $\Omega \approx \omega_c$ and $\Omega \approx 2\omega_c$, the first-order Fourier coefficient was the prominent contributor to the time-resolved dynamics. For the subharmonic resonance at $2\Omega \approx \omega_c$, the second-order Fourier component was found to contribute significantly. This is expected, given that this resonance is sensitive to the second-order Fourier components within the electronic occupation, as seen in Eqs. (80) and (81).

Figure 4 also shows how the simplistic model fails to capture the resonance effects while still capturing the general trend of the phonon occupation. This is understandable, given the simplistic model disregards the driving's effects on the central system's dynamics.

IV. CONCLUSION

In this work we have investigated the periodic driving of a quantum dot with a Floquet nonequilibrium Green's function approach and *GD* approximation. Specifically, the case of sinusoidal driving of the left lead was investigated for a single-level and phonon system.

Particularly interesting for the stability of such driven systems, it was found that driving the lead energies in resonance with the vibrational frequency resulted in increased variations in average position, average momentum, and occupation of the phonon mode. Moreover, while the time-averaged phonon occupation shows an increase in occupation when resonance occurs [see Figs. 3(h) and 4], the time-resolved result [Fig. 3(g)] reveals more pronounced increases in occupation over the period of driving, reflecting the need to analyze
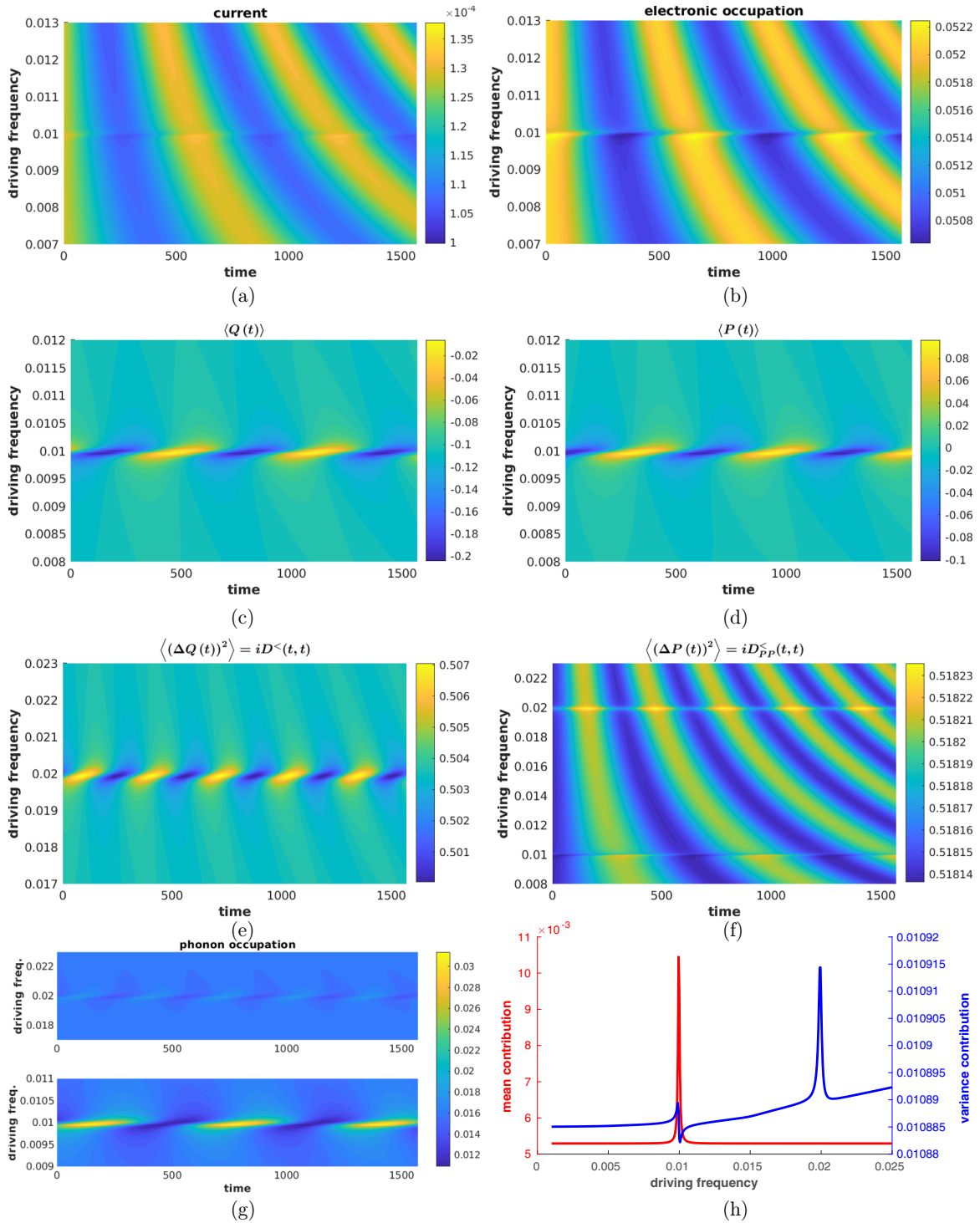
FIG. 3. Figures (a)–(g) plot objects of interest over time, while figure (h) plots the time-averaged contributions to the phonon occupation, as given by Eq. (13). The physical parameters are $\Gamma_L = \Gamma_R = 0.015$, $\epsilon_c = 0.1$, $T = 1.5 \times 10^{-4}$, $\omega_c = 0.01$, $\eta_c = 6 \times 10^{-5}$, $\Delta_L = 0.0015$, and $\lambda_c = 0.01$. Fourier coefficients ranging from–14 to 14 were used in the calculation, with an integrand discretization of 2.5×10^{-5} with bounds of -1 and 1. The convergence was below 10^{-4} for both the electronic and phonon occupation.

time-resolved results when dealing with periodically driven systems.

Also discussed was a simple phenomenological model that was found to replicate the time-averaged observables rather well in regimes away from resonance, particularly when the

driving frequency was smaller than the vibrational frequency, see Fig. 2.

The method presented can be extended to many levels, with the addition of extra sites allowing for investigation of models where phonon modes may couple to many electronic sites or
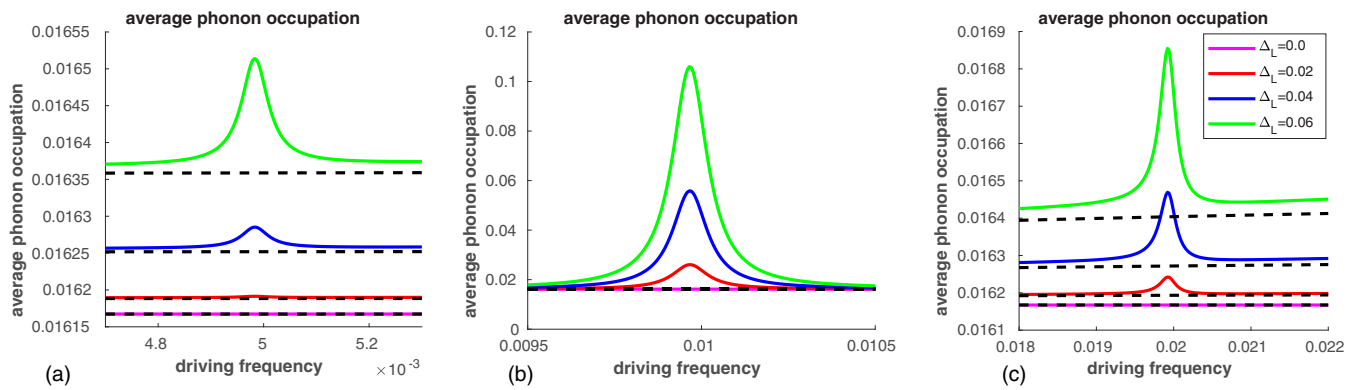
FIG. 4. The time-averaged phonon occupation as driving frequency increases. Here, the driving energies of the left lead, Δ_L, have been varied. Furthermore, the simplistic method has been plotted in dashed black. The other parameters are $\Gamma_L = \Gamma_R = 0.015$, $\epsilon_c = 0.1$, $\eta_c = 6 \times 10^5$, $\omega_c = 0.01$, $\lambda_c = 0.01$, and $T = 1.5 \times 10^{-4}$. The bounds of the integrands were taken at–1 and 1. Fourier coefficients ranging from–8 to 8 were used in the calculation. The uniform grid spacing was 5×10^{-6} for plots (a) and (b), while plot (c) was calculated with 1×10^{-5}. The convergence was below 10^{-4} for both the electronic and phonon occupation.

to the coupling between sites [15]. Furthermore, the effects of different waveforms for the driving could allow for novel means of probing and controlling junction dynamics.

Adding full-counting statistics to the method could allow for the investigation of higher cumulants in the current, including zero-frequency noise [15,30]. This could help answer and motivate questions surrounding the noisiness of signals passed through vibrationally active junctions, an important line of inquiry for functional devices. Additionally, statistics surrounding the phononic occupancies may be of importance, with the average occupations not being enough to evaluate the risk of device failure, given the possibility of large variances in occupation.

This study has made use of self-consistent perturbation theory, allowing small electron-vibrational coupling strengths relative to what is present in many junction architectures. Whether the findings of the investigation follow in stronger settings remains to be seen. However, one can hypothesize that given an increase in electron-vibrational coupling results in more pronounced resonance effects in the present work, the effects of resonance would only become larger in methods able to handle far stronger couplings.

[1] J. C. Cuevas and E. Scheer, *Molecular Electronics*, 2nd ed. (World Scientific, Singapore, 2017).

[2] M. Galperin, M. A. Ratner, and A. Nitzan, J. Chem. Phys. **121**, 11965 (2004).

[3] M. Galperin, M. A. Ratner, and A. Nitzan, Nano Lett. **4**, 1605 (2004).

[4] D. Djukic, K. S. Thygesen, C. Untiedt, R. H. M. Smit, K. W. Jacobsen, and J. M. van Ruitenbeek, Phys. Rev. B **71**, 161402(R) (2005).

[5] O. Tal, M. Krieger, B. Leerink, and J. M. van Ruitenbeek, Phys. Rev. Lett. **100**, 196804 (2008).

[6] S. You, J.-T. Lü, J. Guo, and Y. Jiang, Adv. Phys.: X **2**, 907 (2017).

[7] D. Ryndyk, *Theory of Quantum Transport at Nanoscale: An Introduction*, Springer Series in Solid-State Sciences (Springer International Publishing, Berlin, 2015).

[8] R. J. Preston, V. F. Kershaw, and D. S. Kosov, Phys. Rev. B **101**, 155415 (2020).

[9] J.-T. Lü, M. Brandbyge, and P. Hedegård, Nano Lett. **10**, 1657 (2010).

[10] R. J. Preston, M. F. Gelin, and D. S. Kosov, J. Chem. Phys. **154**, 114108 (2021).

[11] N. Bode, S. V. Kusminskiy, R. Egger, and F. von Oppen, Beilstein J. Nanotechnol. **3**, 144 (2012).

[12] J.-T. Lü, M. Brandbyge, P. Hedegård, T. N. Todorov, and D. Dundas, Phys. Rev. B **85**, 245444 (2012).

[13] V. F. Kershaw and D. S. Kosov, J. Chem. Phys. **153**, 154101 (2020).

[14] M. Galperin, M. A. Ratner, and A. Nitzan, J. Phys.: Condens. Matter **19**, 103201 (2007).

[15] T.-H. Park and M. Galperin, Phys. Rev. B **84**, 205450 (2011).

[16] L. K. Dash, H. Ness, and R. W. Godby, J. Chem. Phys. **132**, 104113 (2010).

[17] S. Maier, T. L. Schmidt, and A. Komnik, Phys. Rev. B **83**, 085401 (2011).

[18] R. Seoane Souto, A. Levy Yeyati, A. Martín-Rodero, and R. C. Monreal, Phys. Rev. B **89**, 085412 (2014).

[19] M. Galperin, A. Nitzan, and M. A. Ratner, Phys. Rev. B **73**, 045314 (2006).

[20] M. Kuperman, L. Nagar, and U. Peskin, Nano Lett. **20**, 5531 (2020).

[21] C. Schinabeck and M. Thoss, Phys. Rev. B **101**, 075422 (2020).

[22] C. R. Peiris, S. Ciampi, E. M. Dief, J. Zhang, P. J. Canfield, A. P. Le Brun, D. S. Kosov, J. R. Reimers, and N. Darwish, Chem. Sci. **11**, 5246 (2020).

[23] Y. Ke, A. Erpenbeck, U. Peskin, and M. Thoss, J. Chem. Phys. **154**, 234702 (2021).

[24] R. Arielly, N. Nachman, Y. Zelinskyy, V. May, and Y. Selzer, J. Chem. Phys. **146**, 092306 (2017).

[25] X. W. Tu, J. H. Lee, and W. Ho, J. Chem. Phys. **124**, 021105 (2006).

[26] J. Trasobares, D. Vuillaume, D. Théron, and N. Clément, Nat. Commun. **7**, 12850 (2016).

[27] P. Haughian, H. H. Yap, J. Gong, and T. L. Schmidt, Phys. Rev. B **96**, 195432 (2017).

[28] M. Ridley, V. N. Singh, E. Gull, and G. Cohen, Phys. Rev. B **97**, 115109 (2018).

[29] M. Ridley, N. W. Talarico, D. Karlsson, N. L. Gullo, and R. Tuovinen, J. Phys. A: Math. Theor. **55**, 273001 (2022).

[30] T. D. Honeychurch and D. S. Kosov, Phys. Rev. B **102**, 195409 (2020).

[31] A. Erpenbeck, L. Götzendörfer, C. Schinabeck, and M. Thoss, Eur. Phys. J.: Spec. Top. **227**, 1981 (2019).

[32] K. Beltako, N. Cavassilas, M. Lannoo, and F. Michelini, J. Phys. Chem. C **123**, 30885 (2019).

[33] M. A. Ochoa, Y. Selzer, U. Peskin, and M. Galperin, J. Phys. Chem. Lett. **6**, 470 (2015).

[34] G. Cabra, I. Franco, and M. Galperin, J. Chem. Phys. **152**, 094101 (2020).

[35] T. D. Honeychurch and D. S. Kosov, Phys. Rev. B **100**, 245423 (2019).

[36] J. Bätge, A. Levy, W. Dou, and M. Thoss, Phys. Rev. B **106**, 075419 (2022).

[37] R. S. Souto, R. Avriller, A. L. Yeyati, and A. Martín-Rodero, New J. Phys. **20**, 083039 (2018).

[38] R. Seoane Souto, R. Avriller, R. C. Monreal, A. Martín-Rodero, and A. Levy Yeyati, Phys. Rev. B **92**, 125435 (2015).

[39] P. Haughian, S. Walter, A. Nunnenkamp, and T. L. Schmidt, Phys. Rev. B **94**, 205412 (2016).

[40] A. Ueda, Y. Utsumi, Y. Tokura, O. Entin-Wohlman, and A. Aharony, J. Chem. Phys. **146**, 092313 (2017).

[41] A. Ueda, Y. Utsumi, H. Imamura, and Y. Tokura, J. Phys. Soc. Jpn. **85**, 043703 (2016).

[42] A. Ueda, O. Entin-Wohlman, and A. Aharony, Phys. Rev. B **83**, 155438 (2011).

[43] R. J. Preston, T. D. Honeychurch, and D. S. Kosov, J. Chem. Phys. **153**, 121102 (2020).

[44] D. Karlsson and R. van Leeuwen, Non-equilibrium Green's functions for coupled fermion-boson systems, in *Handbook of Materials Modeling, Methods: Theory and Modeling*, edited by W. Andreoni and S. Yip (Springer International Publishing, Cham, 2020), pp. 367–395.

[45] M. Schüler, J. Berakdar, and Y. Pavlyukh, Phys. Rev. B **93**, 054303 (2016).

[46] N. Säkkinen, Y. Peng, H. Appel, and R. van Leeuwen, J. Chem. Phys. **143**, 234101 (2015).

[47] H. Haug and A. P. Jauho, *Quantum Kinetics in Transport and Optics of Semiconductors*, Solid-State Sciences Vol. 123 (Springer, Berlin, Heidelberg, 2008).

[48] G. Stefanucci and R. van Leeuwen, *Nonequilibrium Many-Body Theory of Quantum Systems: A Modern Introduction* (Cambridge University Press, Cambridge, England, 2013).

[49] J. Rammer, *Quantum Field Theory of Non-Equilibrium States* (Cambridge University Press, Cambridge, England, 2007).

[50] T. Brandes, Phys. Rev. B **56**, 1213 (1997).

[51] A.-P. Jauho, N. S. Wingreen, and Y. Meir, Phys. Rev. B **50**, 5528 (1994).

[52] G. Platero and R. Aguado, Phys. Rep. **395**, 1 (2004).

[53] U. Peskin, Fortschr. Phys. **65**, 1600048 (2017).